Growth, structure, and transport properties of thin (>10 nm) *n*-type microcrystalline silicon prepared on silicon oxide and its application to single-electron transistor

T. Kamiya[a)]
Materials and Structure Laboratory, Tokyo Institute of Technology, 4259 Nagatsuta, Midori-ku, Yokohama 226-8503, Japan, Microelectronics Research Centre, Cavendish Laboratory, University of Cambridge, Madingley Road, Cambridge CB3 0HE, United Kingdom, and CREST, JST, 3-13-11 Shibuya, Tokyo 150-0002, Japan

K. Nakahata
Graduate School, Tokyo Institute of Technology, 4259 Nagatsuta, Midori-ku, Yokohama 226-8502, Japan

Y. T. Tan and Z. A. K. Durrani
Microelectronics Research Centre, Cavendish Laboratory, University of Cambridge, Madingley Road, Cambridge CB3 0HE, United Kingdom and CREST, JST, 3-13-11 Shibuya, Tokyo 150-0002, Japan

I. Shimizu
Graduate School, Tokyo Institute of Technology, 4259 Nagatsuta, Midori-ku, Yokohama 226-8502, Japan

(Received 14 November 2000; accepted for publication 6 March 2001)

Microcrystalline silicon (μc-Si:H) thin films were prepared at 300 °C on glass. Their structure and transport properties were studied in a wide range of film thickness ranging from 10 nm to 1 μm. The crystal fraction increases monotonously from ~64% to ~100% as film thickness increases. Electron mobility first increases with increasing film thickness at thicknesses smaller than 50 nm but saturates at larger thickness. This mobility behavior is explained by percolation transport through crystalline grains. These results are different from those obtained with preferentially oriented polycrystalline silicon films. It is related to the difference in the microstructure evolution in which subsequent film growth is influenced by the growth surface structure. A single-electron transistor fabricated in 30-nm-thick μc-Si:H exhibits Coulomb blockade effects at 4.2 K. This result indicates that amorphous phases which exist between crystalline grains behave as tunnel barrier for electrons.
© *2001 American Institute of Physics.* [DOI: 10.1063/1.1368164]

I. INTRODUCTION

Poly-/micro-crystalline silicon (poly-/μc-Si:H) thin films have been used for various devices such as thin film solar cells and thin film transistor (TFT) arrays for flat panel displays.[1–6] Plasma-enhanced chemical vapor deposition (PECVD) is not only a common and simple technique employed in the fabrication of these silicon-based devices, it also provides the ability to control the film microstructure such as the grain size and the grain boundary structure. This feature makes it suitable for the development of materials for novel quantum effect devices such as single-electron transistors (SETs).

Solar cells and TFTs are usually fabricated in poly-/μc-Si:H films deposited on nonsingle-crystalline substrates such as polycrystalline transparent conductive oxide, metal or plastic sheets. This reduces the substrate cost and allows for the use of large-area substrates that may lead to the development of new devices such as flexible solar cells and future sheet computers. In addition, TFTs and SETs can be prepared on silicon-on-insulator substrates for higher operation speed and better electrical isolation. However, thin amorphous silicon (a-Si:H) or amorphous rich layers (referred to as incubation layers) are formed during the initial growth of poly-/μc-Si:H on nonsingle-crystalline substrates, which deteriorates device performance. Thus many attempts have been made to improve film crystallinity during the initial growth of poly-/μc-Si:H on glass.[7–10]

In our previous work, we have reported on high crystallinity, high quality poly-Si:H films prepared on glass from SiF_4 and H_2 gas mixtures, where a fluorinated source gas enhances crystallization and crystallite growth.[11] The film microstructures including the grain orientation are controlled by selecting appropriate deposition conditions,[12,13] which would lead to suitable device applications. For example, (220) oriented poly-Si can be grown at small gas flow ratios (e.g., $SiF_4/H_2<30/10$ sccm) at 300 °C. It has rather large surface roughness and lateral grain size. Due to more pronounced natural light scattering at the rough film surface and grain boundaries, this material has an efficient light-trapping function that results in higher apparent optical absorption in solar cell photoactive layers.[14,15] The (400) oriented poly-Si can be grown at a higher gas flow ratio of 60/3 sccm at 300 °C and it has a smoother surface, higher quality crystalline grains and a larger carrier mobility.[13] This material may be used for high performance TFT.[5] It is also possible to grow μc-Si:H with high crystallinity (crystal fraction >60%) at temperatures as low as 50 °C with small SiF_4/H_2

[a)]Electronic mail: kamiya@iem.titech.ac.jp

Downloaded 08 Oct 2004 to 131.111.8.103. Redistribution subject to AIP license or copyright, see http://jap.aip.org/jap/copyright.jsp

ratios.[16] In this case, the grains are randomly oriented and the grain size is rather small (<30 nm in size). Such small grain sizes may find novel applications in quantum effect devices. We note that quantum confinement effects in such small grain size silicon-based material have been observed as a blueshift in photoluminescence.[17]

Poly-/μc-Si:H prepared at low temperatures on glass can have an inhomogeneous structure and structural and transport properties such as grain size, crystalline fraction, orientation fluctuation and carrier mobilities can be a strong function of film thickness[18–23] In addition, the film structure and transport properties can be changed by doping. This indicates that it is necessary to study film microstructure and transport properties at a thickness and doping concentration that is used in a specific device application.

The structural and transport properties of thick (>1 μm) poly-/μc-Si:H have been studied intensively as these films are required for solar cells.[1,4] In contrast, TFTs and SETs require the film thickness to be less than 100 nm.[6] Although many studies exist on nucleation and growth of μc-Si:H,[24–28] we did not find a detailed study on transport properties in relation to the structure for very thin films targeted at SET applications.

In this article, we focus on the structural and transport properties of μc-Si:H films of thickness from 10 nm to 1 μm. These films were prepared by very-high-frequency PECVD (VHF CVD) and the deposition condition was optimized to prepare thin μc-Si:H films on glass with high crystallinity. In addition, we fabricated a SET to examine the potential of this material in a quantum effect device application.

II. EXPERIMENT

A. Fabrication of μc-Si:H films

The μc-Si:H thin films were prepared by 100 MHz VHF CVD from a $SiF_4/H_2/SiH_4$ gas mixture (see Refs. 11 and 16 for details). After optimizing the deposition condition, a gas flow rate of $SiF_4/H_2/SiH_4=30/40/0.25$ sccm and a growth temperature of 300 °C were used to obtain a high crystalline fraction for thin films. Most of the films were doped using PH_3, 1% diluted with H_2, at a concentration of $[PH_3]/[SiH_4]=2\%$ to facilitate Hall effect measurement and electrical characterization of SETs. The VHF power was 40 W and the reactor pressure was 200 mTorr. Corning 7059 glass was used for structural characterizations and Hall effect measurements, 150-nm-thick SiO_2 thermally grown on n-type single-crystalline silicon (c-Si) was used as the substrate in the preparation of the SET.

B. Fabrication of SETs

A lateral double side-gated nanowire was defined in the μc-Si:H film using electron-beam lithography on polymethyl methacrylate resist and reactive ion etched in a 1:1 plasma of $SiCl_4$ and CF_4 (see Ref. 29 for details). The nanowire was 1 μm long and 60 nm wide and the side gates to the nanowire separation were 120 nm (Fig. 1). Finally, aluminum was deposited to form ohmic contacts to the μc-Si:H film after removing the surface oxide layer in buffered HF.

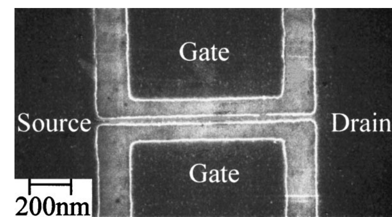

FIG. 1. SEM micrograph of double-gated SET with dimensions of 60 nm width and 1 μm length.

C. Structural and electrical characterization

The film structures were studied using x-ray diffraction (XRD) analysis and reflection high-energy electron diffraction (RHEED) analysis. The crystalline fraction was estimated from the c-Si to a-Si:H TO phonon band peak area ratio in the Raman spectrum[30] and the grain size was estimated using a microcrystalline model.[31,32] The pseudodielectric function (imaginary part will be referred to as $\langle \epsilon_2 \rangle$) was measured by a spectral ellipsometer (SE) and analyzed using a multilayer optical model to determine the crystalline fraction for thin films.[33] Surface morphology was observed by atomic force microscopy (AFM). Hall effect measurements were performed in a temperature range of 90–420 K. The electrical characteristic of the SET was measured at 4.2 K.

III. RESULTS AND DISCUSSIONS

A. Film structure

Figure 2 shows the XRD profiles of the n-type μc-Si:H film. An XRD profile for an undoped μc-Si:H film prepared with the same conditions is shown for comparison. The undoped μc-Si:H exhibits (220) preferential orientation while the n-type μc-Si:H films exhibit (111) preferential orientation if the film thickness is larger than 0.35 μm. This result is consistent with that reported by Kakinuma, i.e., high doping of PH_3 tends to promote (111) oriented grain growth.[34] When the film exhibits (220) orientation, Scherrer diameters estimated from 111 (D_{111}) and 220 (D_{220}) diffraction peak

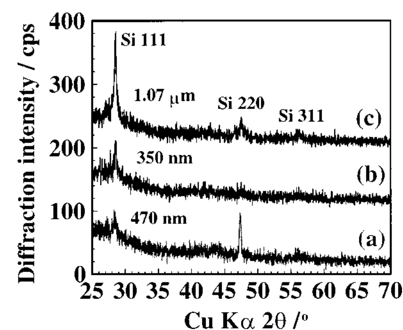

FIG. 2. XRD profiles of undoped μc-Si:H (a) and n-type μc-Si:H [(b), (c)]. The doping concentration is $[PH_3]/[SiH_4]=2\%$ in source gas. Numbers in figure indicate film thickness.

Downloaded 08 Oct 2004 to 131.111.8.103. Redistribution subject to AIP license or copyright, see http://jap.aip.org/jap/copyright.jsp

TABLE I. Scherrer diameter estimated from 111 (D_{111}) and 220 (D_{220}) diffraction widths.

	Thickness/μm	D_{111}/nm	D_{220}/nm
Undoped	0.47	17	54
n-type	0.35	26	15
n-type	1.07	29	18

widths are 17 and 54 nm, respectively, for the 0.47-μm-thick film (Table I). In contrast, the 1.07-μm-thick *n*-type μc-Si:H film has larger D_{111} value of 29 nm and smaller D_{220} value of 18 nm. It is known that inhomogeneous strain makes the D_{220} value smaller than the D_{111} value because it increases the diffraction peak widths at larger diffraction angles. However, this is not the case for the undoped μc-Si:H because the D_{220} value is larger than the D_{111} value. These results indicate that the grain size depends on crystallite orientation and that crystallites with the major preferential orientation of the film have a large grain height. It is thought that the 220 diffraction in the *n*-type μc-Si:H is attributed to randomly oriented crystallites because the 220–311 diffraction intensity ratio is almost the same as that obtained with randomly oriented silicon powder. It should be noted that the grain size in the *n*-type μc-Si:H film does not change dramatically with film thickness as seen in Table I.

RHEED images (Fig. 3) provide structural information for thinner films. Broad continuous diffraction rings are observed with a hallow bright background for 10-nm-thick μc-Si:H. This suggests that the film contains randomly oriented microcrystalline and amorphous phases. The diffraction ring width becomes sharper as the film thickness increases to 25 nm, indicating that the grain size increases during film growth in this thickness range. In the RHEED image of the 1.07 μm film, we can see spotty diffractions superimposed on the continuous diffraction rings. This indicates that the film has 111 oriented grains near the surface. Therefore, we conclude that the 111 oriented grains appear after the film thickness exceeds 25 nm.

For film thickness less than 220 nm, the AFM images in Fig. 4 show that the lateral grain size increases as the film thickness increases. However, the lateral grain size does not change markedly at a larger thickness (Fig. 5). This result is consistent with the variation of the perpendicular grain size

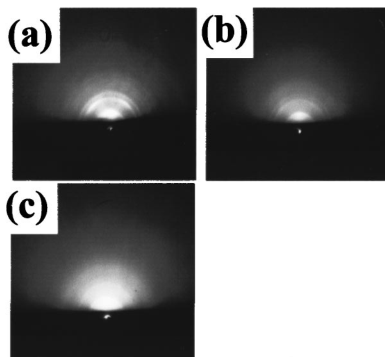

FIG. 3. RHEED images of *n*-type μc-Si:H as a function of film thickness. Film thicknesses are 1.07 μm (a), 25 nm (b), and 10 nm (c).

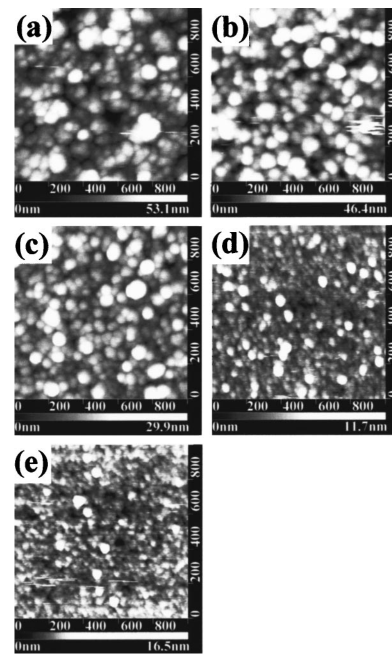

FIG. 4. AFM images of *n*-type μc-Si:H as a function of film thickness. Thicknesses are 1.07 μm (a), 350 nm (b), 220 nm (c), 25 nm (d), and 10 nm (e). Scan area is 1 μm×1 μm.

obtained by XRD (D_{220}), in which the D_{220} value did not change between 0.35 and 1.07 μm thicknesses. The root mean square (rms) roughness increases proportionally with $d^{(0.40\pm0.03)}$ (*d*: film thickness), indicating a limited diffusion assisted-film growth process.[35]

Crystalline fraction and grain size were evaluated using Raman scattering spectrum. In the case of 1.07-μm-thick film, the profile was interpreted as a mixture of microcrystalline silicon grains ~7.0 and ~2.6 nm in size. An amorphous phase peak was not necessary to explain the profile. When the film thickness is smaller than the penetration depth of the pumping laser light (300–500 nm for 514.5 nm wavelength), the precise evaluation of the crystalline fraction by the Raman spectrum is difficult because the profile includes a significant signal from the glass substrate. By subtracting the signal from substrate, the crystal fraction was estimated to be 70% for 50-nm-thick film and it was found that the film contained crystalline grains ~5.4 and ~3.0 nm in size. The size of the larger grains is smaller than in the 1.07-μm-thick film, agreeing with the AFM result (Fig. 4). However, the

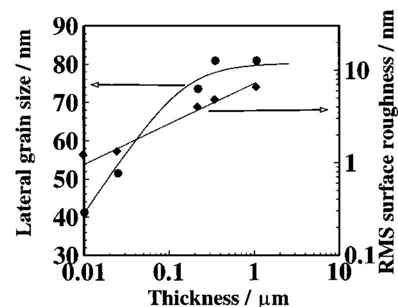

FIG. 5. Lateral grain size (circles) and rms surface roughness (diamonds) evaluated from AFM images.

Downloaded 08 Oct 2004 to 131.111.8.103. Redistribution subject to AIP license or copyright, see http://jap.aip.org/jap/copyright.jsp

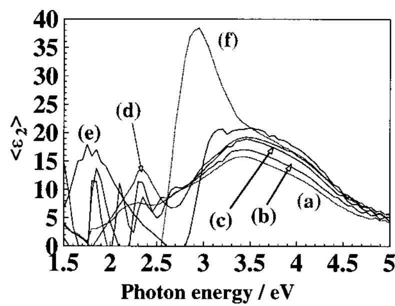

FIG. 6. Pseudo-dielectric function $\langle \epsilon_2 \rangle$ of μc-Si:H as a function of film thickness. Thicknesses are 1.07 μm (a), 350 nm (b), 220 nm (c), 100 nm (d), 50 nm (e), and 25 nm (f).

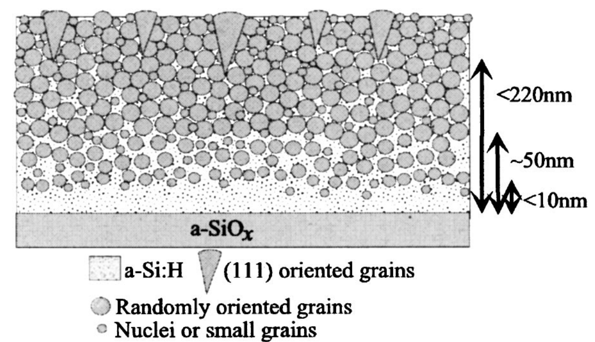

FIG. 8. Schematic illustration of film microstructure.

absolute values of the grain sizes measured by Raman analysis are much smaller than those observed by the AFM. We have reported a similar discrepancy between scanning electron microscopy (SEM) observation and XRD analysis for (220) oriented poly-Si.[13] This is because the large grains observed by SEM consist of smaller single-domain crystallites which are observed by XRD: i.e., the larger grains have small secondary structures. Similarly, it is thought that the Raman analysis provides grain sizes of the smaller single-domain crystallites and that the μc-Si:H contains small grains with size of $\sim$3 nm independent of film thickness, suggesting that new nuclei are formed at/near the growth surface during the film deposition. It is possible that P-related impurity sites form preferential nucleation sites and enhance the nucleation process.

For more precise determination of the crystalline fraction, $\langle \epsilon_2 \rangle$ was measured by SE (Fig. 6). We observe broad peaks around 3.4 and 4.1 eV, attributed to band-to-band transition absorptions in crystalline silicon. The broad nature of these peaks indicates that the grain size is small. Using a multilayer optical model comprising microcrystalline silicon, amorphous silicon and void, we evaluate the crystalline fraction to be $\sim$64% for 50-nm-thick film and $\sim$100% for film thickness increasing to 1.07 μm (Fig. 7). This agrees well with the Raman results.

We can now summarize the film growth process (Fig. 8). The grains are initially randomly oriented but change to (111) preferential orientation as the film grows, due to the high P doping. The crystalline grains grow in height and in diameter as the film thickness increases up to $\sim$50 nm but their sizes do not change markedly at larger thickness. Approximately 30% of amorphous phase remains in 50-nm-thick film. The crystalline fraction increases to $\sim$100% for 1.07-μm-thick films. All μc-Si:H films contain crystalline grains with different sizes and the size of the small grains does not change dramatically with film thickness.

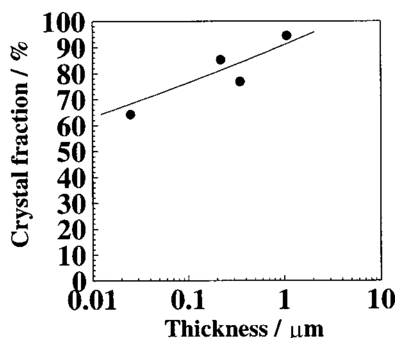

FIG. 7. Crystalline fraction evaluated by the SE analysis.

B. Transport properties

Figure 9 shows the conductivity, electron mobility and carrier concentration of the films evaluated by Hall effect measurements. It is worth noting that all the films do not exhibit any double anomaly of Hall voltage sign as reported in amorphous semiconductors.[36] This indicates that even the 10-nm-thick μc-Si:H film has drift carriers and the scattering length is long enough for the Hall effect measurement

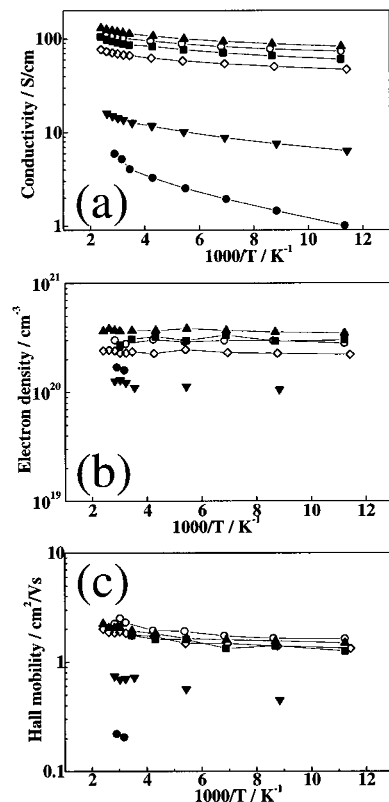

FIG. 9. Conductivity (a), mobility (b) and electron density (c) as a function of temperature and film thickness. Thicknesses are 1.07 μm (diamonds), 220 nm (open circles), 100 nm (triangles), 50 nm (squares), 25 nm (reverse triangles), and 10 nm (closed circles).

Downloaded 08 Oct 2004 to 131.111.8.103. Redistribution subject to AIP license or copyright, see http://jap.aip.org/jap/copyright.jsp

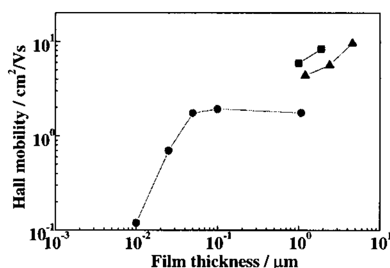

FIG. 10. Room temperature Hall mobility as a function of film thickness. Those obtained for (220) and (400) oriented poly-Si are also shown for comparison (see Ref. 22). Circles: μc-Si:H, triangles: (220) oriented poly-Si, squares: (400) oriented poly-Si.

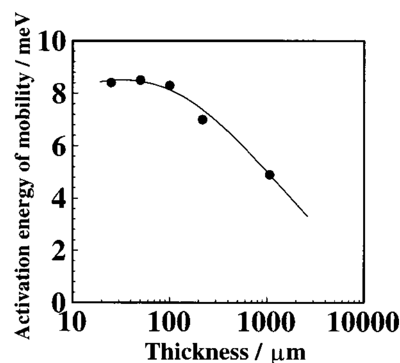

FIG. 11. Hall mobility activation energy as a function of film thickness.

condition. Although some scattering is found in the measured values due to the difficulty in an accurate measurement of the Hall voltage with high impedance samples, the room temperature carrier density only decreases from $3.7 \times 10^{20}/\mathrm{cm}^3$ to $1.1 \times 10^{20}/\mathrm{cm}^3$ with decreasing film thickness while the conductivity falls markedly by one order of magnitude. The carrier density does not show obvious temperature dependence, indicating a degenerate semiconductor. The decrease in the carrier density in thin films may be attributed to the lower ionization efficiency of P in an amorphous phase than in crystalline grains. Neither the mobility nor the electron density change greatly when the film thickness is larger than 50 nm. At a thickness less than 50 nm, the mobility falls rapidly by one order of magnitude, which is the main reason for the large decrease in conductivity.

C. Growth mechanism of μc-Si:H and relationship between film microstructure and transport properties

Figure 10 summarizes the relationship between room temperature Hall mobility and film thickness. The results obtained on (220) or (400) preferentially oriented poly-Si films are also shown in the figure for comparison. The Hall mobility of the μc-Si:H increases with film thickness for thickness less than 50 nm and saturates at $\sim 1.8\ \mathrm{cm}^2/\mathrm{V\,s}$ when the film thickness is greater than 50 nm. The initial increase in mobility is explained by the increases in crystalline fraction and grain size, which enables carrier percolation transport path through the crystalline grains. For thinner films, carriers move through amorphous phases between the crystalline grains, resulting in a low mobility. The activation energy of Hall mobility at room temperature is almost constant at a thickness less than 100 nm while it decreases with film thickness at larger thicknesses (Fig. 11), which supports this idea.

It is interesting that Hall mobilities of (220) or (400) preferentially oriented films exhibit different behavior, i.e., they increase monotonously with film thickness. As Nakahata *et al.* report, Hall mobility has a good correlation with the lateral grain size measured by SEM and the lateral growth in preferentially oriented poly-Si occurs together with a decrease in orientation fluctuation.[12,22] Their results imply that the chemical bonding structure at the growth surface affects the structure of the subsequently grown film. In contrast, it is thought that the growth of the randomly oriented μc-Si:H is not affected by the growth surface structure under the deposition condition used because the perpendicular grain size of the μc-Si:H measured by XRD (D_{220}) is much smaller than the film thickness and also smaller than those measured in the (220) or (400) preferentially oriented poly-Si.[3,37] This may result in a saturation of lateral and perpendicular grain size as well as Hall mobility observed in the μc-Si:H films.

As Kamiya *et al.* report, the growth of the (400) oriented poly-Si depends significantly on the growth surface structure.[13,38] Under conditions where (220) oriented poly-Si films are grown, the grain height tends to decrease with an increasing hydrogen mixing ratio, which is similar to the result obtained with a SiH_4/H_2 system.[39] In low-temperature PECVD system using H_2 and SiH_4 gases, the majority of the growth surface is covered with hydrogen under high hydrogen mixing ratio conditions. In the SiF_4/H_2 system, the hydrogen coverage is thought to decrease with an increasing SiF_4/H_2 ratio, due to the extraction of the hydrogen by F-related radicals and a decrease in hydrogen radical density in plasma. The lower hydrogen coverage forms reactive sites such as dangling bonds at the growth surface, making the epitaxial-like subsequent film growth easier. In contrast, high hydrogen coverage forms chemically inactive growth surfaces, and also makes new nuclei formation at the growth surface easier because the deposition precursor diffusion length becomes longer.[40] This model agrees with the Raman results, which suggested that new nuclei were formed at/near the growth surface during film growth. In addition, unlike the case of preferentially oriented poly-Si, where lateral grain growth is enhanced by the driving force to decrease orientation fluctuation,[12] randomly oriented grains do not have a driving force for lateral grain growth after each grain is in contact with neighboring grains. Thus the grain size is determined by the nucleus density in the randomly oriented μc-Si:H case. We conclude that this growth mechanism is caused by a high hydrogen mixing ratio and results in smaller grain sizes.

D. Single-electron charging effect

Figure 12 shows the schematic band diagram for thin (<50 nm) μc-Si:H deduced from the Hall measurement results. From Figs. 10 and 11, we deduced that the percolation through crystalline grains began at a film thickness of $\sim$50 nm, suggesting that some crystalline grains were isolated by

Downloaded 08 Oct 2004 to 131.111.8.103. Redistribution subject to AIP license or copyright, see http://jap.aip.org/jap/copyright.jsp

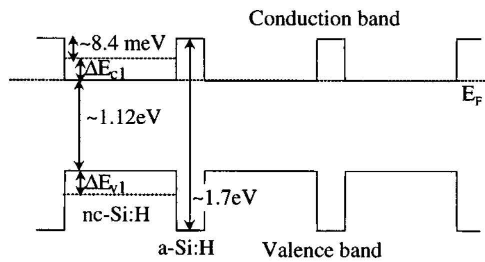

FIG. 12. Schematic diagram of electronic states in 50-nm-thick *n*-type μc-Si:H. ΔE_{c1} and ΔE_{v1} indicate first energy levels formed due to carrier confinement in quantum dots. The ΔE_{c1} is almost zero for 5-nm-diam quantum dot (after Ref. 41).

thin amorphous phases from neighboring crystalline grains. The Fermi level in a-Si:H depends on doping concentration, defect density and amorphous network structure and the dopant concentration is thought to be different in between crystalline grains and in a-Si:H. Thus it is difficult to estimate the band offset of the conduction band. However, the activation energy of the Hall mobility is ~8.4 meV at room temperature for 50 nm-thick μc-Si:H. This value decreases to 5 meV for thicker films, where the dominant carrier transport path is thought to be percolating (Fig. 11). Carrier density did not show obvious temperature dependence. Thus, we may think that the Fermi level is located very close to the conduction band edge in crystalline grains and the band offset of the conduction band is ~8.4 meV. This band offset value corresponds to 97 K, which is high enough for carrier confinement at 4.2 K. In addition, the μc-Si:H contains small crystalline grains ~3 nm in size.

These results indicate that films near 50 nm thickness have either large conductivity or small crystalline grains isolated by thin amorphous tissues with a wider band gap than that of crystalline silicon. These features would be suitable to observe single-electron charging effects. Figure 13 shows the source-drain current–voltage characteristics of a SET fabricated in a 30-nm-thick μc-Si:H film. It exhibits nonlinear current–voltage characteristics with staircase-like structure at 4.2 K (shown more clearly from the first derivative). The average staircase period is ~26 mV. Figure 14 shows the current oscillations with respect to gate voltage. Oscillations with different periods are superimposed in the characteristics with periods of 30, 60, 200, 370, 490 and 800 mV. We may

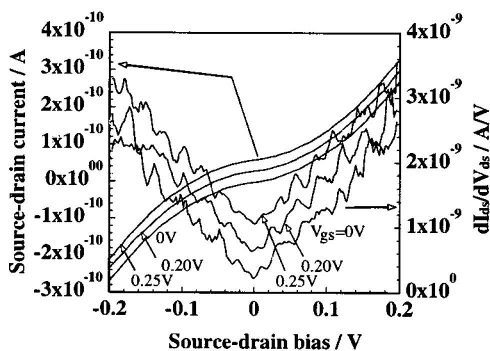

FIG. 13. Source-drain $I-V$ characteristics and the first derivative (dI_{ds}/dV_{ds}) of the SET. The V_{gs} indicates gate-source bias voltage.

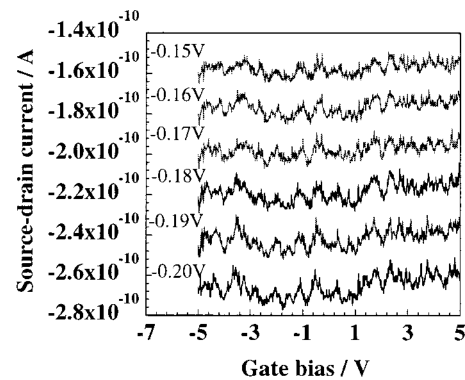

FIG. 14. Gate-bias current oscillation of the SET. Source-drain voltage V_{ds} was swept from −0.20 to −0.15 V with steps of 10 mV (V_{ds}s are indicated in the figure).

attribute these oscillations to different sized islands. These results are attributed to the Coulomb blockade effects in a multiple-tunnel junction and multiple-islands system with different size islands. Since the SET nanowire has a large dimension of 60 nm width×1 μm length, the Coulomb blockade characteristics are complicated and not distinct. Further study on the SET with smaller dimension has been ongoing.

IV. CONCLUSION

We have studied the structural and transport properties of *n*-type thin μc-Si:H prepared by low-temperature PECVD. The film orientation changed from a random to a (111) preferential orientation with film growth. The crystalline grains grew in height and in diameter when the film thickness was less than 50 nm. The grain size did not change greatly at larger film thicknesses. A large content of amorphous phase (~30%) remained in the 50-nm-thick film and the crystalline fraction increased to ~100% for the 1.07-μm-thick film. The films contained crystalline grains with different sizes, and the smaller grain size was ~3 nm, suggesting that new nuclei were formed during the film growth due to large hydrogen mixing ratio.

Electron mobility increased with increasing film thickness at thickness up to 50 nm and saturated at larger film thickness. This behavior was very different from those obtained in preferentially oriented poly-Si films, which could be related to the difference in the microstructure evolution originated from different deposition condition and growth surface structure. Hall effect measurements suggested that the percolation threshold appeared at a thickness of ~50 nm. We speculate that some crystalline grains in films are isolated by thin amorphous phases with a conduction band offset of ~8.4 meV.

A SET fabricated in the 30-nm-thick μc-Si:H displayed Coulomb blockade effects and gate-bias current oscillations at 4.2 K and we believe that the amorphous phases form tunnel barriers for electrons in this device.

These results demonstrate that high crystallinity μc-Si:H can be prepared using PECVD at 300 °C with a high hydrogen mixing ratio. We believe that this is a promising material for future novel devices such as SETs.

Downloaded 08 Oct 2004 to 131.111.8.103. Redistribution subject to AIP license or copyright, see http://jap.aip.org/jap/copyright.jsp

ACKNOWLEDGMENTS

This work is supported by the Japan Science and Technology Corporation (JST) through the core research for evolutional science and technology (CREST) project NeoSilicon. The authors would like to express their appreciation to Professor H. Ahmed at the Microelectronics Research Centre of the Cavendish Laboratory, University of Cambridge, for his helpful discussion and advice for this work.

[1] J. Meier *et al.*, J. Non-Cryst. Solids **227–230**, 1250 (1998).
[2] J. Yang, A. Banerjee, and S. Guha, Appl. Phys. Lett. **70**, 2975 (1997).
[3] C. Beneking, B. Rech, S. Wieder, O. Kluth, H. Wagner, W. Frammelsberger, R. Geyer, P. Lechner, H. Rubel, and H. Schade, Thin Solid Films **351**, 241 (1999).
[4] K. Yamamoto, M. Yoshimi, T. Suzuki, Y. Tawada, Y. Okamoto, and A. Nakajima, Mater. Res. Soc. Symp. Proc. **507**, 131 (1998).
[5] T. Nagahara, K. Fujimoto, N. Kohno, Y. Kashiwagi, and H. Kakinoki, Jpn. J. Appl. Phys., Part 1 **31**, 4555 (1992).
[6] T. Sameshima, Appl. Surf. Sci. **96–98**, 352 (1996).
[7] J. Zhou, K. Ikuta, T. Yasuda, T. Umeda, S. Yamasaki, and K. Tana, J. Non-Cryst. Solids **227–230**, 857 (1998).
[8] S. Ishihara, D. He, and I. Shimizu, Jpn. J. Appl. Phys., Part 1 **33**, 51 (1994).
[9] T. Kamiya, K. Ro, C. M. Fortmann, and I. Shimizu, Jpn. J. Appl. Phys., Part 1 **38**, 5762 (1999).
[10] A. Heya, A. Masuda, and H. Matsumura, Appl. Phys. Lett. **74**, 2143 (1999).
[11] K. Nakahata, K. Ro, A. Suemasu, T. Kamiya, C. M. Fortmann, and I. Shimizu, Jpn. J. Appl. Phys., Part 1 **39**, 3294 (2000).
[12] T. Kamiya, K. Nakahata, A. Miida, C. M. Fortmann, and I. Shimizu, Thin Solid Films **337**, 18 (1999).
[13] T. Kamiya, K. Nakahata, K. Ro, C. M. Fortmann, and I. Shimizu, Jpn. J. Appl. Phys., Part 1 **38**, 5750 (1999).
[14] K. Ro, K. Nakahata, T. Kamiya, C. M. Fortmann, and I. Shimizu, J. Non-Cryst. Solids **266**, 1088 (2000).
[15] K. Yamamoto, T. Suzuki, M. Yoshimi, and A. Nakajima, Jpn. J. Appl. Phys., Part 2 **36**, L569 (1997).
[16] T. Kamiya, K. Nakahata, K. Ro, C. M. Fortmann, and I. Shimizu, Mater. Res. Soc. Symp. Proc. **557**, 513 (1999).
[17] Y. Hirano, F. Sato, N. Saito, M. Abe, S. Miyazaki, and M. Hirose, J. Non-Cryst. Solids **266–269**, 1004 (2000).
[18] M. Otobe and S. Oda, Jpn. J. Appl. Phys., Part 1 **31**, 1948 (1992).
[19] H. Matsumura, Y. Tashiro, K. Sasaki, and S. Furukawa, Jpn. J. Appl. Phys., Part 2 **33**, L1209 (1994).
[20] A. Fejfar, N. Beck, H. Stuchlikova, N. Wyrsch, P. Torres, J. Meier, A. Shah, and J. Kocka, J. Non-Cryst. Solids **227–230**, 1006 (1998).
[21] S. Brehme, P. Kanschat, and W. Fuhs, Mater. Res. Soc. Symp. Proc. **609**, A.32.2.1 (2000).
[22] K. Nakahata, A. Miida, T. Kamiya, C. M. Fortmann, and I. Shimizu, Thin Solid Films **337**, 45 (1999).
[23] A. Masuda, R. Iiduka, A. Heya, C. Niikura, and H. Matsumura, J. Non-Cryst. Solids **227–230**, 987 (1998).
[24] K. Ikuta, K. Tanaka, S. Yamasaki, K. Miki, and A. Matsuda, Appl. Phys. Lett. **65**, 1760 (1994).
[25] H. Fujiwara, Y. Toyoshima, M. Kondo, and A. Matsuda, J. Non-Cryst. Solids **266–269**, 38 (2000).
[26] R. i Cabarocas, N. Layadi, B. Drevillon, and I. Solomon, J. Non-Cryst. Solids **198–200**, 871 (1996).
[27] Y. Okazaki, S. Miyazaki, and M. Hirose, J. Non-Cryst. Solids **266–269**, 54 (2000).
[28] S. Moniruzzaman, T. Inokuma, Y. Kurata, S. Takenaka, and S. Hasegawa, Thin Solid Films **337**, 27 (1999).
[29] Y. T. Tan, Z. A. K. Durrani, and H. Ahmed, J. Appl. Phys. **89**, 1262 (2001).
[30] T. Kaneko, K. Onisawa, M. Wakagi, Y. Kita, and T. Minemura, Jpn. J. Appl. Phys., Part 1 **32**, 4907 (1993).
[31] H. Richter, Z. P. Wang, and L. Ley, Solid State Commun. **39**, 625 (1981).
[32] Z. Sui, P. P. Leong, and I. P. Herman, Appl. Phys. Lett. **60**, 2086 (1992).
[33] D. E. Aspnes and J. B. Theeten, Phys. Rev. B **20**, 3292 (1979).
[34] H. Kakinuma, J. Vac. Sci. Technol. A **13**, 2310 (1995).
[35] M. Kondo, T. Ohe, K. Saito, T. Nishimiya, and A. Matsuda, J. Non-Cryst. Solids **227–230**, 890 (1998).
[36] K. Morigaki, *Physics of Amorphous Semiconductors* (World Scientific, Singapore, 1999), p. 123.
[37] T. Kamiya, Y. Maeda, K. Nakahata, T. Komaru, C. M. Fortmann, and I. Shimizu, J. Ceram. Soc. Jpn. **107**, 1099 (1999) (in Japanese).
[38] T. Kamiya, K. Nakahata, C. M. Fortmann, and I. Shimizu, J. Non-Cryst. Solids **266–269**, 120 (2000).
[39] E. Vallat-Sauvain, U. Kroll, J. Meier, N. Wyrsch, and A. Shah, J. Non-Cryst. Solids **266–269**, 125 (2000).
[40] A. Matsuda, Thin Solid Films **337**, 1 (1999).
[41] S. Y. Ren and J. D. Dow, Phys. Rev. B **45**, 6492 (1992).

Downloaded 08 Oct 2004 to 131.111.8.103. Redistribution subject to AIP license or copyright, see http://jap.aip.org/jap/copyright.jsp